Int. J. Electrochem. Sci., 12 **(2017)** 9007 – 9016, doi: 10.20964/2017.10.05

International Journal of
ELECTROCHEMICAL
SCIENCE
www.electrochemsci.org

Corrosion and Electrochemical Impedance Properties of Ti Alloys as Orthopaedic Trauma Implant Materials

Xinqing Guo[1],*Huiming Shi*[2] *and Lifeng Xi*[3*]

[1] Department of Orthopaedics, Luoyang Dongfang Hospital, The Third Affiliated Hospital of Henan University of Science and Technology, Luoyang, Henan, 471003, P.R. China
[2] Ward 1, Department of Traumatic Orthopedics, Hanzhong Central Hospital, Hanzhong, Shaanxi, 723000, P.R.China
[3] Department of Joint Surgery, Yellow River Sanmenxia Hospital, Sanmenxia, Henan, 472000, P.R.China
[*]E-mail: lifengluoyang@foxmail.com

Received: 31 May 2017 / *Accepted:* 26 July 2017 / *Published:* 12 September 2017

In this study, Ti–24Nb–4Zr–8Sn, a titanium alloy used in orthopaedic trauma implants, was studied for its electrochemical corrosion performance (in weight percent) in a phosphate buffered saline (PBS) solution at 37 °C using electrochemical impedance spectroscopy (EIS), open-circuit potential (OCP) and potentiodynamic polarization strategies. A Ti–6Al–4V sample was compared with commercially pure titanium. The experimental data indicated that the spontaneous passivation of the specimens occurred as soon as they were immersed in the electrolyte. The passive region of the Ti–24Nb–4Zr–8Sn sample was wider than those of the Ti–6Al–4V and pure titanium samples. Additionally, the corrosion current density of the Ti–24Nb–4Zr–8Sn sample was as low as that of pure titanium.

Keywords: Ti based alloy; Orthopaedic trauma implant; Electrochemical impedance; Corrosion behaviour; Open circuit potential

1. INTRODUCTION

Orthopaedic trauma implants are medical devices for substituting a missing bone or joint to support damaged bone. Titanium alloys and stainless steel are used to fabricate the medical implant and provide strength. Meanwhile, the plastic coating formed on the implant functions as an artificial cartilage. As an orthopaedic operation, internal fixation consists of the surgical implementation of implants to repair a bone. Plates, screws, rods and pins are the frequently used medical implants for anchoring fractured bones during the healing process. Titanium and alloys based on it are extensively utilized in orthopaedic applications due to their numerous advantages, including desirable biocompatibility, high corrosion resistance, suitable mechanical features and a high strength-to-weight

ratio [1-3]. The high corrosion resistance of titanium and titanium-based alloys in chloride-containing solutions and other aggressive environments results from the thickness (several nanometres) of the naturally formed passive TiO_2 layer. Nevertheless, this thin layer does not have the capacity to deal with the essential biochemical requirements among others [4-6].

It has been widely accepted that the corrosion resistance of titanium alloys (biomedical grade) *in vitro* is high. However, according to several reports, the accumulation of titanium in surrounding tissues could be observed after the Ti was dissolved and released [7-11]. The use of Ti-based implant alloys causes concern, since the potential release of the V, Zr, Al and other metallic ions into the tissues surrounding the implant would lead to unfavourable reactions and excessive tissue degradation. Additionally, the titanium surface exhibits undesirable chemical reactivity that results in the spontaneous formation of a hydroxyapatite layer and a direct bond with living bone tissue [12-15]. Hence, the fixation rate of the implant was expected to be low, and the implant could be applied for a prolonged time period, gradually degrading over the healing period. Another important factor for titanium bio-implants is their tribological performance, which can lead to problems during real-world use [16, 17]. Understanding the location where the implant is attacked by the synergistic effect of wear and corrosion (tribocorrosion) (i.e., in hip/knee and dentistry replacements) is an important problem. Therefore, eliminating the adverse effects of tribocorrosion on the biocompatibility of Ti bio-implants (by increasing the wear resistance) was of vital importance. Additionally, the properties of the surface are of vital importance to bio-implants in contact with human body. Therefore, surface modification is one potential strategy for enhancing the bioactivity, biocompatibility, tribocorrosion and corrosion of these systems based on the time and function of implantation [18].

In recent years, several studies have proposed Ti–24Nb–4Zr–8Sn (by weight percent), a novel multifunctional β-type titanium alloy, and have applied it to biomedical fields [19-21]. In comparison with previously reported alloys, this alloy exhibited a more desirable compromise between a low elastic modulus and high strength. The corrosion performance of this biomaterial in the human body is of vital importance. As an ultra-complex electrolyte, the human body environment contains substantially erosive species that facilitate the electrochemical mechanisms of hydrolysis and corrosion. There have been extensive studies on the corrosion performance of titanium and titanium alloys [22-29]. These previous reports concluded that surface oxide film dissolution and corrosion are the two primary mechanisms for ions released into the body. Substantial amounts of ions released from a prosthesis could cause mechanical failure of the implant device through adverse biological reactions.

In this work, a Ti–24Nb–4Zr–8Sn sample was investigated to assess its corrosion behaviour in a simulated physiological environment. The electrochemical performance of the sample was studied in PBS at 37 °C using OCP, EIS and potentiodynamic polarization. Additionally, the Ti–6Al–4V and commercially pure titanium (CP-Ti) samples were compared with the proposed sample.

2. EXPERIMENTS

2.1. Samples and reagents

The substrates were commercially pure titanium and Ti-6Al-4V samples with a surface area of 10 mm × 10 mm. An ingot (nominal chemical composition: Ti–24Nb–4Zr–8Sn (wt.%)) was prepared

from pure Zr, pure Nb, pure Ti and a TiSn master alloy using the vacuum arc-melting method. After hot-forging at 800 °C to a 50 mm slab and heat-treatment for 60 min at 750 °C, this ingot was air-cooled. An electrical spark was used for cutting the 10 mm × 10 mm × 5 mm rectangular plates. Unfavourable effects was prevented by connecting a copper wire onto the specimen surface via a brass nut. Afterwards, all specimens were placed into a plastic tube. After being sealed with an epoxy resin, this tube had a cross-sectional area of 1.0 cm^2. This was followed by mechanical polishing of the specimen's surfaces using 57–10 μm SiC papers, ultrasonic cleaning in acetone, ethanol and distilled water for 10 min each and drying in a cold air stream. Next, SiC papers were used to grind the obtained specimens to obtain 1200-grit products followed by mechanical polishing with Al_2O_3 powder (diameter: 0.5 μm). In contrast, the substrates were cleaned under ultrasonic treatment in ethanol and distilled water, and etched in a solution of HF/HNO_3 and distilled water (1:10:30 wt. ratio) for 90 s at ambient temperature. After washing in distilled water, the as-etched specimens were immersed in an anodizing solution.

2.2. Characterizations

Characterizations were performed in an aerated PBS solution (pH 7.4) that contained KH_2PO_4 (0.2 g), $Na_2HPO_4 \cdot 12H_2O$ (2.9 g), KCl (0.2 g) and NaCl (8 g) in 1 L of water. The measurements were conducted in the freshly prepared PBS at 37 °C (constant). All electrochemical measurements were conducted on a computer–controlled potentiostat (model IviumStat – XR), and the data were recorded. A conventional triple-electrode configuration was used, where the reference electrode was saturated calomel, and the counter electrode was a large platinum sheet.

The OCP experiment was performed for 5.0×10^4 s starting when the electrode was immersed into the electrolyte. After immersion in PBS for 60 min, the potentiodynamic polarization profiles were recorded, where the OCP exhibited a range of potentials from −500 mV to 2500 mV (against SCE) (scan rate: 0.6 mV/s). A sinusoidal perturbation of 10 mV was applied at the OCP to perform the EIS measurements, where the impedance spectra were recorded (frequency sweep range: 100 kHz to 10 mHz) in logarithmic increments. Bote and Bote plots were recorded after immersing the specimens into the solution for 60 min.

3. RESULTS AND DISCUSSION

Fig. 1 shows the changes in the OCP for the CP-Ti, Ti–6Al–4V and Ti–24Nb–4Zr–8Sn alloys after various immersion durations in PBS. A positive shift was observed for the potential of these samples, suggesting that protective passive films formed on their surfaces. After an initial increase in its potential, the Ti–24Nb–4Zr–8Sn sample showed a gradual decrease in it OCP, which became stable ca. -0.17 V after 1×10^4 s, indicating that the passive film had stabilized. Compared with the proposed sample, the CP-Ti exhibited a similar OCP profile, apart from the peak potential during the initial stage. However, the Ti–6Al–4V sample showed different OCP profiles at the initial stage (up to

5.9×10^3 s) before a stable state was observed ca. −0.20 V. Thus, the stable OCP values of the three samples were nearly the same.

The Ti and Ti-based alloys exhibited high corrosion resistance, since a protective oxide film spontaneously formed on their surfaces. XPS analysis has shown that this amorphous oxide film consists of three layers: TiO, Ti_2O_3 and TiO_2 [30]. Once the material is contact with the electrolyte, the transformation from TiO or Ti_2O_3 to TiO_2 will occur on the electrode/electrolyte interface [31]. The electrode corrosion resistance increased until it eventually reached a plateau. The titanium alloy showed a decrease in its anodic dissolution current as the corrosion resistance increased. The OCP is an anodic and cathodic reaction that is determined by the non-equilibrium electrode potential. Thus, in accordance with the electro-neutrality theory, a gradual shift of the OCP towards the positive direction was observed with a decrease in the anodic current, leading to an adequately low cathodic current to balance the decreased anodic current. Once a comparatively stable value was maintained for the corrosion resistance of the oxide film on the titanium alloy, a stable state was observed for the anodic current and the OCP.

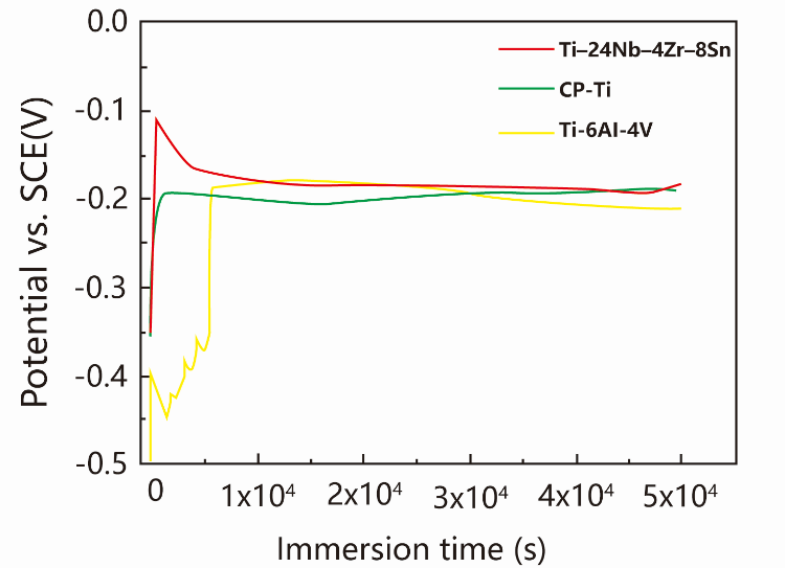

Figure 1. Open circuit potential as a function of time in the PBS solution at 37 °C.

The CP-Ti, Ti–6Al–4V and Ti–24Nb–4Zr–8Sn specimens in PBS at 37 °C were characterized via their potentiodynamic polarization profiles, shown in Fig. 2, to investigate the intensity, continuity and stability of the passive Ti oxide film. It can be clearly observed that all of the specimens displayed typical active-passive behaviour and were characterized by direct transfer from the Tafel area to the passive area. As indicated in the profiles, CP-Ti, Ti–24Nb–4Zr–8Sn and Ti–6Al–4V displayed the corrosion potentials (E_{corr}) of −0.38 V, −0.52 V and −0.67 V (against SCE), respectively. The cathodic and anodic branches in these polarization profiles were used to calculate the corrosion current densities (I_{corr}) using a Tafel analysis. The Ti–6Al–4V sample exhibited an I_{corr} value of ca. 0.017 μA/cm^2. However, the CP-Ti and Ti–24Nb–4Zr–8Sn samples displayed slightly higher I_{corr} values, 0.035 and 0.037 μA/cm^2 (nearly equivalent to each other), respectively. A characteristic activation polarization

was observed for the Ti–24Nb–4Zr–8Sn sample within the potential range of −0.53 to −0.12 V (against SCE), indicating that the potential was linearly related with the current density. The Ti–24Nb–4Zr–8Sn alloy shows a wider passivation region than CP-Ti and Ti–6Al–4V, as evidenced by the current remaining constant as the potential increased, which indicated that the passive film formed on the surface of the Ti–24Nb–4Zr–8Sn alloy is integral to preventing corrosion. Compared with the Ti–6Al–4V and CP-Ti samples, the Ti–24Nb–4Zr–8Sn sample displayed a higher I_{pp} value of ~3.03 μA/cm^2, further indicating its different properties. The Ti–24Nb–4Zr–8Sn sample showed a slight increase in the current density when the potential was beyond ~1.2 V (against SCE). Repassivation was observed for the Ti–24Nb–4Zr–8Sn sample when the potential was further increased to 1.4 V (against SCE). This increase may be related to the formation of TiO_2 from TiO and Ti_2O_3 [32]. When the potential increased to as high as 2.5 V (against SCE), the Ti–24Nb–4Zr–8Sn sample showed no breakdown potential, indicating that this sample was highly resistant to local corrosion. However, the Ti–6Al–4V and CP-Ti sample exhibited different performances as follows. As the potential increased to 0.5 V (against SCE), a significant increase in the current density was observed, which then transferred to the repassivation area after the appearance of an activation peak. Table 1 shows the values of the aforementioned parameters.

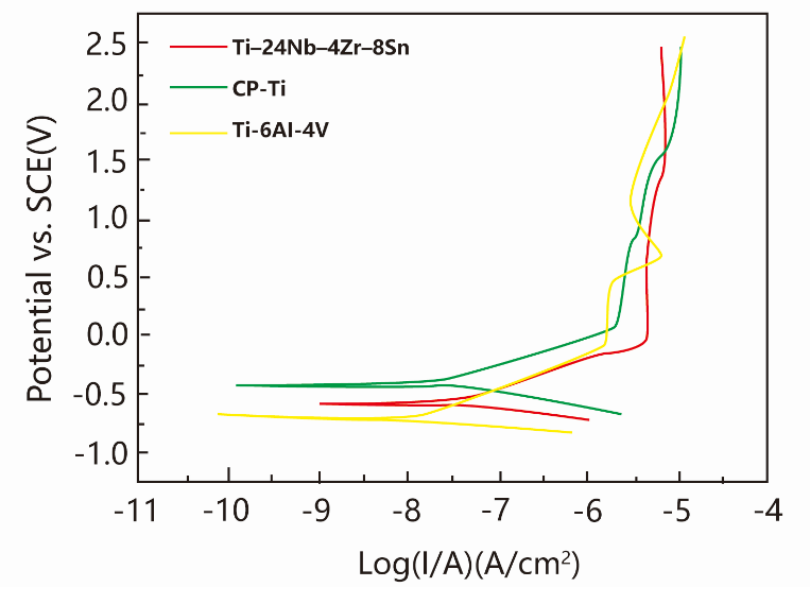

Figure 2. Potentiodynamic polarization curves in the PBS solution at 37 °C.

Table 1. Corrosion parameters of Ti–24Nb–4Zr–8Sn, CP-Ti and Ti–6Al–4V in the PBS solution at 37 °C.

Specimens	I_{corr} (μA/cm^2)	E_{corr} (V)	I_p (μA/cm^2)
Ti–24Nb–4Zr–8Sn	0.037	−0.52	3.03
Ti-6Al-4V	0.020	−0.67	2.24
CP-Ti	0.035	−0.38	1.85

The passivation features of the Ti–24Nb–4Zr–8Sn sample were more desirable than those of the Ti–6Al–4V and CP-Ti samples, and the corrosion rate of the Ti–24Nb–4Zr–8Sn sample was comparable to the CP-Ti sample, as indicated in the polarization profiles and by the active dissolution parameters (Table 1).

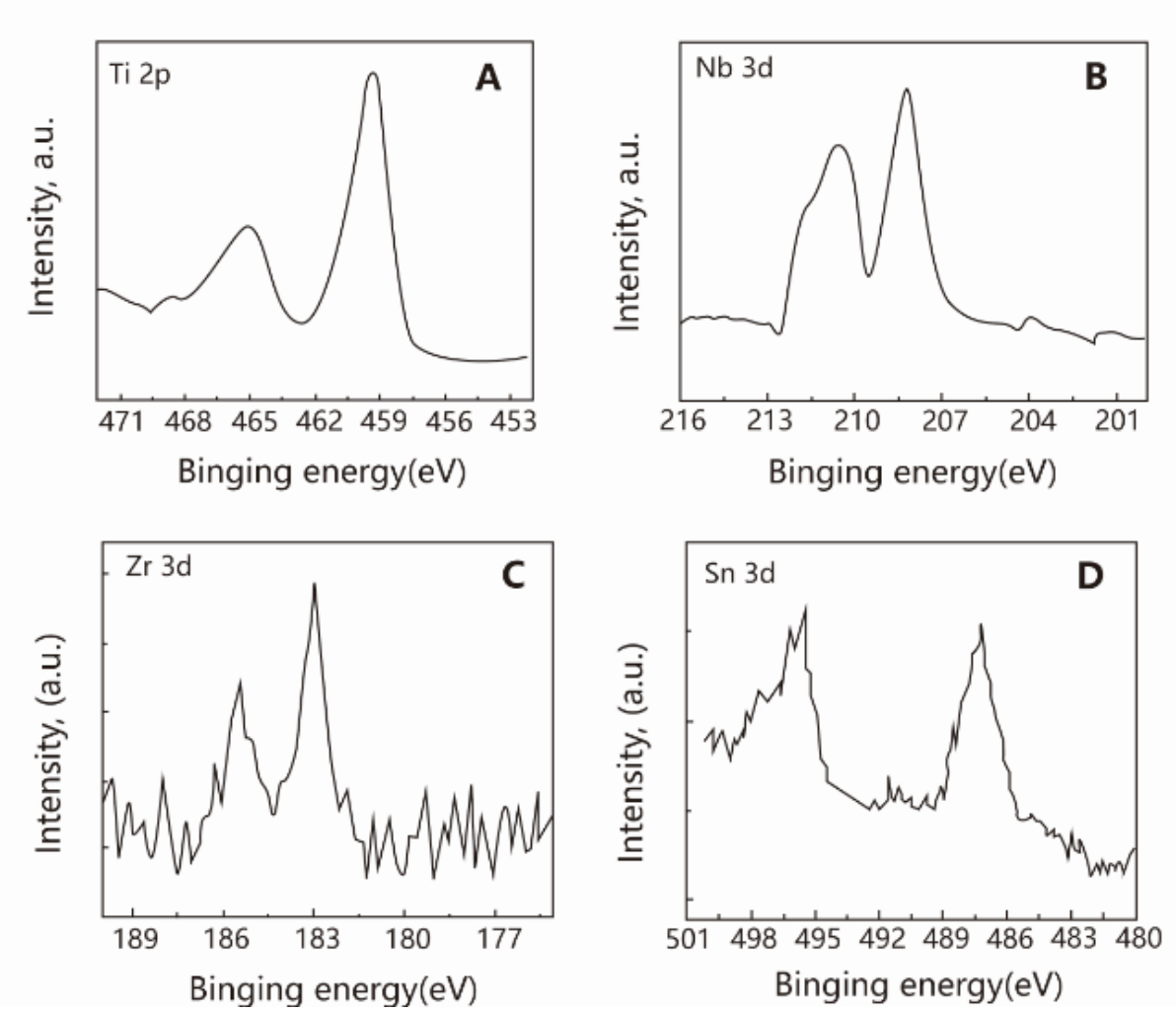

Figure 3. XPS spectra of Ti–24Nb–4Zr–8Sn alloy in the PBS solution at 37 °C: (A) Ti 2p, (B) Nb 3d, (C) Zr 3d (D) Sn 3d.

This phenomenon was possibly caused by the composition of the protective oxide film produced on the Ti–24Nb–4Zr–8Sn surface. The compositions of the protective oxide films were investigated using XPS. As shown in Fig. 3, the Sn 3d signal, Zr 3d signal, Nb 3d signal and Ti 2p signal were observed at 486.6, 183.2, 206.5 and 458.4 eV, respectively, and the binding energies of these signals suggested that the major constituents of the passive film of the Ti–24Nb–4Zr–8Sn sample were Nb_2O_5 and TiO2 with some SnO_2 and ZrO_2. The effect of the alloying constitutions on the electrochemical performance of titanium alloys has been investigated in some reports. The Ti–6Al–7Nb sample was determined to be less susceptible to corrosion than the Ti–6Al–4V sample, indicating that Nb can promote the passivation of titanium alloys. In fact, the alloying addition-induced structural changes to the TiO_2 oxide determine the effects of the alloying composition on the passivation features of the samples. Nb could enhance the stoichiometricity and corrosion resistance of the oxide film

formed on the Ti–24Nb–4Zr–8Sn sample because the Nb^{5+} cations in the crystal lattice of titanium oxide could reduce the concentration of anion vacancies formed due to lower titanium oxidation states such as Ti^{3+} and Ti^{2+} [33]. Compared with the Ti–6Al–4V and CP-Ti samples, Ti–24Nb–4Zr–8Sn showed better passivation features in PBS. Yu et al. [34] concluded that the alloying addition of Nb results in an improved resistance to active dissolution in acidic solutions and an enhanced passivation relative to pure titanium. The previous studies also noted the combinational contributions of alloying elements; for example, both Nb and Zr additions favour the formation of strong covalent bands between nearby neighbouring Ti, Nb and Zr sites by the sharing of unpaired d-level electrons [35].

As indicated in Fig. 4, the impedance spectra of the CP-Ti, Ti–24Nb–4Zr–8Sn and Ti–6Al–4V samples were characterized via Bode and Nyquist plots. All the Nyquist plots in Fig. 4A shows an incomplete semicircle, corresponding to a near capacitive response. The Ti–24Nb–4Zr–8Sn sample showed a semicircle with a smaller diameter compared with that of the Ti–6Al–4V sample, and the diameter of the former was nearly equivalent to that of the CP-Ti sample. The Bode magnitude plots (Fig. 4B) showed two different regions for the three samples. A flat portion with a slope of ca. 0 was observed in the high frequency range (10^3–10^5 Hz), corresponding to the electrolyte resistance. A wide frequency range of 10^{-1} to 10^2 Hz (phase angle: −85°) was suggested for both the CP-Ti and Ti–24Nb–4Zr–8Sn samples in the Bode phase plots (Fig. 4B), possibly since a single passive oxide film was formed on the surface [35]. As indicated in Fig. 4B, a decrease in the phase angle was observed in the high frequency range of 10^3 to 10^5 Hz that was ascribed to the response of the electrolyte's resistance. A decrease of the phase angle down to −40° was observed in the low frequency range (10^{-2} to 10^{-1} Hz), which was attributed to the contribution from the passive film's resistance. The change in phase angle caused by the frequency fluctuations in the Ti–24Nb–4Zr–8Sn sample was different from that caused by the frequency fluctuation in the Ti–6Al–4V sample. We recorded two phase angle maximums with one each in the high and low frequency ranges. This difference was possibly because of the duplex passive film structure that formed on the Ti–6Al–4V sample. In the region below 10^3 Hz, the spectra displayed a linear slope of approximately −1, which is characteristic of capacitive behaviour in the passive film [36].

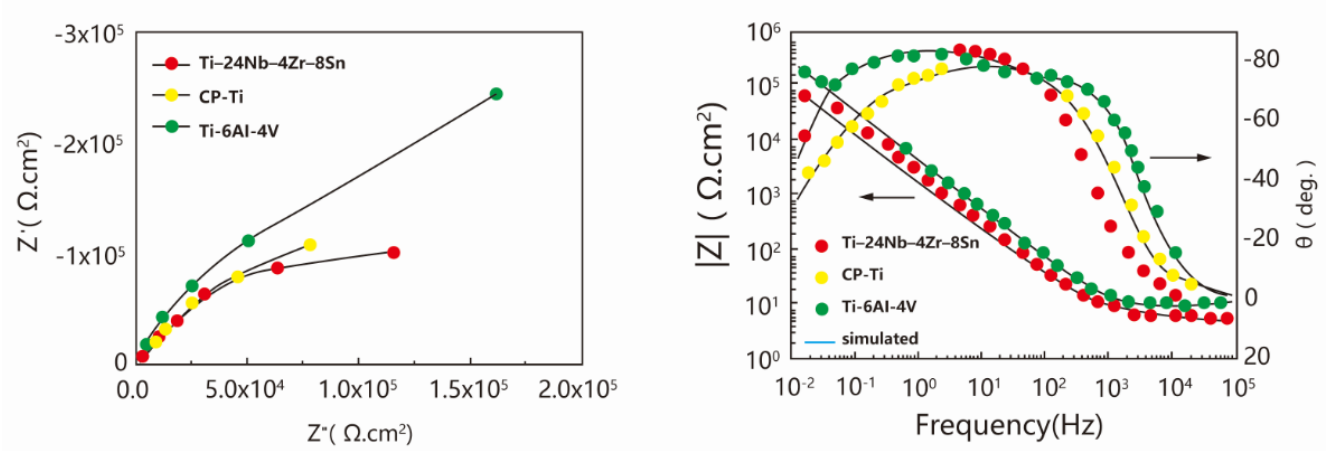

Figure 4. (A) Nyquist plots in the PBS solution at 37 °C. (B) Bode plots in the PBS solution at 37 °C, in which the open symbols are the experimental results and the solid curves are the modeling results.

Equivalent circuits with one or more time constants were used to model the alteration of the impedance with the frequency. The interfacial performances of the CP-Ti and Ti–24Nb–4Zr–8Sn samples (where a single passive film was formed) was fitted by a $R_s(Q_1R_1)$ model with only one time constant (Fig. 5A), as shown with the EIS results in Fig. 4. With respect to the above model, R_s, R_1 and Q_1 represented the electrolyte resistance, the resistance of passive film and the constant phase element (CPE) of the passive film. In theory, a slope of −1 and a phase shift of −90° were expected for an ideal dielectric material, but these did not appear for the barrier films. Since this was considered with respect to the CPE, the fitting was performed using CPE rather than the capacitance *C*. In fact, the CPE impedance was expressed as

$$Z_{CPE} = [Cn(jw)]^{-1}$$

where *C*, *w*, *n*, referred, respectively, to the ideal capacitor-associated capacitance, the angular frequency and the factor indicating the deviation from the ideal capacitive performance associated with adsorption effects, surface inhomogeneity, and roughness factors. The surface layer exhibited a performance almost equal to that of an ideal capacitor, with *n* approaching ca. 1. The fitting of the EIS data for the Ti–6Al–4V sample was performed using a $R_s(Q_1R_1)(Q_2R_2)$ model with two time constants, where $R_{s,}$ footnote 1, and footnote 2 referred to the electrolyte resistance, the porous outer layer, and the compact inner layer, respectively. Table 2 shows the numerical results and the chi-square value-expressed errors. The chi-square value ranged from 0.02 to 0.04, suggesting an acceptable agreement.

Table 2. Electrical parameters of the equivalent circuits obtained by fitting the experimental results of EIS data together with the chi-square values.

Materials	Rs (Ω/cm^2)	R1 (MΩ/cm^2)	Q1 (μF/cm^2)	n1	R_2 (MΩ cm^2)	Q2 (μF/cm^2)	n2	Chi-square
Ti–24Nb–4Zr–8Sn	11.3	0.23	58.1	0.914	—	—	—	0.04
CP-Ti	10.4	0.21	50.4	0.924	—	—	—	0.03
Ti-6Al-4V	6.8	0.0002	35.6	0.851	0.53	28.7	0.933	0.02

With respect to the Ti–24Nb–4Zr–8Sn sample, the resistance (R_1) and capacitance (Q_1) of its passive film were 0.23 MΩ cm^2 and 58.1 μF/cm^2 (similar to the values obtained for the CP-Ti sample), respectively (Table 2). A highly stable film formed on the Ti–24Nb–4Zr–8Sn sample in the test electrolyte, as evidenced by the high R_1 value and the low Q_1 value. A near capacitive performance was observed for this passive film, as suggested by the *n* value of 0.914. Thus, a noble electrochemical corrosion performance could be concluded the Ti–24Nb–4Zr–8Sn sample, corresponding to the comparatively low corrosion rates obtained in the polarization measurement. The equivalent circuit used in the present work has already been used to describe the Ti–6Al–4V alloy, resulting in similar fitted values [37, 38].

The passive film that formed on the Ti–6Al–4V sample in PBS was composed of double layers, as indicated by the developed model, $R_s(Q_1R_1)(Q_2R_2)$. The exponent of Q_2 (n_2) was 0.933, suggesting a high R_2 resistance and a near-capacitive performance, which possibly indicated the formation of a

compact inner layer. The Ti–35Nb sample showed slightly varying impedance parameters [39], suggesting that the inner and outer layers may provide corrosion protection. As indicated in the comparison of the EIS characterizations of these three specimens in PBS at 37 °C, the barrier layer of the Ti–6Al–4V sample displayed the highest resistance compared with those of the CP-Ti and Ti–24Nb–4Zr–8Sn samples. The co-existence of an inner barrier and an outer porous layer could make the specimens more corrosion resistant than a single film. The Ti–6Al–4V sample had a porous layer measuring ~2.5 nm thick and a barrier measuring ~3 nm. The latter value was higher than those of the other samples using the same test electrolyte.

4. CONCLUSIONS

In this study, the spontaneous formation of protective passive films on the surfaces of CP-Ti, Ti–24Nb–4Zr–8Sn, and Ti–6Al–4V samples could be observed upon immersion in PBS at 37 °C. The passivation behaviour of the Ti–24Nb–4Zr–8Sn sample was more desirable than the other samples, and this sample displayed a comparable corrosion rate to the CP-Ti sample. The concentration of the defects present in the passive film of the proposed sample was decreased by the formation of Nb^{5+} cations, which also enhanced its stability by improving its corrosion resistance.

References

1. J. Chen, F. Yan, B. Chen and J. Wang, *Materials and Corrosion*, 64 (2013) 394.
2. S. Tamilselvi, V. Raman and N. Rajendran, *Journal of Applied Electrochemistry*, 40 (2010) 285.
3. R. Narayanan and S. Seshadri, *Corrosion Science*, 50 (2008) 1521.
4. I. Park, T. Woo, M. Lee, S. Ahn, M. Park, T. Bae and K. Seol, *Metals and Materials International*, 12 (2006) 505.
5. M. Golozar, K. Raeissi and M. Fazel, *Journal of Materials Engineering and Performance*, 23 (2014) 1270.
6. M. Diamanti and M. Pedeferri, *Corrosion Science*, 49 (2007) 939.
7. H. Song, M. Kim, G. Jung, M. Vang and Y. Park, *Surface and Coatings Technology*, 201 (2007) 8738.
8. B. Bozzini, P. Carlino, L. D'urzo, V. Pepe, C. Mele and F. Venturo, *Journal of Materials Science: Materials in Medicine*, 19 (2008) 3443.
9. X. Liu, P. Chu and C. Ding, *Materials Science and Engineering: R: Reports*, 47 (2004) 49.
10. A. Fekry, *RSC Advances*, 6 (2016) 20276.
11. S. Esfahani, M. Andani, N. Moghaddam, R. Mirzaeifar and M. Elahinia, *Journal of Materials Processing Technology*, 238 (2016) 22.
12. X. Fan, B. Feng, Y. Di, X. Lu, K. Duan, J. Wang and J. Weng, *Appl. Surf. Sci.*, 258 (2012) 7584.
13. E. Szesz, B. Pereira, N. Kuromoto, C. Marino, G. de Souza and P. Soares, *Thin Solid Films*, 528 (2013) 163.
14. T. Jun, G. Sernicola, F. Dunne and T. Britton, *Materials Science and Engineering: A*, 649 (2016) 39.
15. C. Chan, S. Lee, G. Smith, G. Sarri, C. Ng, A. Sharba and H. Man, *Appl. Surf. Sci.*, 367 (2016) 80.
16. A. Yetim, *Surface and Coatings Technology*, 205 (2010) 1757.
17. A. Yetim, A. Celik and A. Alsaran, *Surface and Coatings Technology*, 205 (2010) 320.

18. W. Chrzanowski, *Journal of Achievements in Materials and Manufacturing Engineering*, 31 (2008) 203.
19. Y. Hao, S. Li, S. Sun, C. Zheng, Q. Hu and R. Yang, *Applied Physics Letters*, 87 (2005) 091906.
20. Y. Hao, S. Li, S. Sun and R. Yang, *Materials Science and Engineering: A*, 441 (2006) 112.
21. Y. Hao, S. Li, S. Sun, C. Zheng and R. Yang, *Acta Biomaterialia*, 3 (2007) 277.
22. C. Kuphasuk, Y. Oshida, C. Andres, S. Hovijitra, M. Barco and D. Brown, *The Journal of Prosthetic Dentistry*, 85 (2001) 195.
23. V. Alves, R. Reis, I. Santos, D. Souza, T. Goncalves, M. Pereira-da-Silva, A. Rossi and L. Da Silva, *Corrosion Science*, 51 (2009) 2473.
24. M. Popa, I. Demetrescu, S. Suh, E. Vasilescu, P. Drob, D. Ionita and C. Vasilescu, *Bioelectrochemistry*, 71 (2007) 126.
25. Y. Kwon, H. Seol, H. Kim, K. Hwang, S. Lee and K. Kim, *Journal of Biomedical Materials Research Part B: Applied Biomaterials*, 73 (2005) 285.
26. H. Ahn, M. Kim, H. Seol, J. Lee, H. Kim and Y. Kwon, *Journal of Biomedical Materials Research Part B: Applied Biomaterials*, 79 (2006) 7.
27. C. Sedarat, M. Harmand, A. Naji and H. Nowzari, *Journal of Periodontal Research*, 36 (2001) 269.
28. S. Takemoto, M. Hattori, M. Yoshinari, E. Kawada and Y. Oda, *Biomaterials*, 26 (2005) 829.
29. Y. Okazaki and E. Gotoh, *Biomaterials*, 26 (2005) 11.
30. J. Pouilleau, D. Devilliers, F. Garrido, S. Durand-Vidal and E. Mahé, *Materials Science and Engineering: B*, 47 (1997) 235.
31. C. Marino, E. de Oliveira, R. Rocha-Filho and S. Biaggio, *Corrosion Science*, 43 (2001) 1465.
32. M. Popa, I. Demetrescu, E. Vasilescu, P. Drob, A. Lopez, J. Mirza-Rosca, C. Vasilescu and D. Ionita, *Electrochimica Acta*, 49 (2004) 2113.
33. M. Metikoš-Huković, A. Kwokal and J. Piljac, *Biomaterials*, 24 (2003) 3765.
34. Y. Steven, J. Scully and C. Vitus, *Journal of the Electrochemical Society*, 148 (2001) B68.
35. A. Shukla, R. Balasubramaniam and S. Bhargava, *Intermetallics*, 13 (2005) 631.
36. A. Hodgson, Y. Mueller, D. Forster and S. Virtanen, *Electrochimica Acta*, 47 (2002) 1913.
37. V. Alves, R. Reis, I. Santos, D. Souza, T. Goncalves, M. Pereira-da-Silva, A. Rossi and L. Da Silva, *Corrosion Science*, 51 (2009) 2473.
38. S. Tamilselvi, V. Raman and N. Rajendran, *Electrochimica Acta*, 52 (2006) 839.
39. A. Cremasco, W. Osório, C. Freire, A. Garcia and R. Caram, *Electrochimica Acta*, 53 (2008) 4867.